Modifying the performance kinetics in the shell-and-multi tube latent heat storage system via dedicated finned tubes for building applications

Mohamed Ahmed Said[1], Hakim S. Sultan Aljibori[2], Jasim M. Mahdi[3],
Hayder Ibrahim Mohammed[4], Pouyan Talebizadehsardari[5,*], Amir Keshmiri[6,*]

[1] Architectural Engineering Department, College of Engineering, University of Ha'il, P.Box 2440, Ha'il City, Saudi Arabia
[2] College of Engineering, University of Warith Al-Anbiyaa, Karbala 56001, Iraq
[3] Department of Energy Engineering, University of Baghdad, Baghdad 10017, Iraq
[4] Department Of Cooling And Air Conditioning Engineering, Imam Ja'afar Al-Sadiq University, Baghdad, Iraq
[5] Power Electronics, Machines and Control (PEMC) Research Group, University of Nottingham, Nottingham, U.K.
[6] School of Engineering, University of Manchester, Manchester, UK

* Corresponding authors

Email: pouyan.talebizadehsardari2@nottingham.ac.uk; a.keshmiri@manchester.ac.uk

Abstract

Phase change materials (PCMs) offer significant potential for building energy management, but are limited by poor heat transfer rates. This study investigates charging/discharging performance optimization of a shell-and-multi-tube heat storage system using high-enthalpy PCM (RT70HC) with differentiated fin configurations. The key novelty of the work lies in its thorough examination of geometric mutations within this system, specifically targeting building energy applications. A validated numerical model simulated charging and discharging processes, comparing finned and plain tube designs. Key performance metrics analyzed here include melting times, heat storage rates, phase transition velocities, and temperature profiles. Results reveal the finned tube design enables a 268% higher heat storage rate (1421 W vs 387 W) and 74.5% faster melting time (196 mins vs 770 mins) compared to the plain tube. Detailed analysis of the 10-hour charging process exposes intricate thermal stratification patterns. The inclusion of dedicated discharging finned tubes significantly enhances heat distribution. During the 20-hour discharge, heat transfer rates decrease from 2000 W to 100 W, providing crucial insights into solidification dynamics. These quantified findings highlight the potential of optimized finned tube arrays to substantially improve thermal performance of shell-and-multi-tube heat storage systems for building energy applications.

Keywords: Computational fluid dynamics, Phase change materials, Shell-and-tube heat exchanger, Geometric fin designs, Energy storage optimization.

1. Introduction

Phase change materials (PCMs) are increasingly utilized in latent-heat thermal energy storage (LHTES) systems due to their exceptional energy-saving capability [1, 2], superior energy storage performance [3, 4], and nearly constant temperature during phase transition [5, 6]. However, a major drawback of PCMs for LHTES is their low thermal conductivity, which hinders effective heat transfer and charging/discharging rates [7]. To address this issue, various heat transfer enhancement techniques have been explored, nanoparticles [8, 9], geometric modifications and optimizations [10-12] , mechanical vibration [13], and porous foams [14, 15]. Their integration into tube-based LHTES configurations, such as shell-and-tube designs, has shown promising improvements to system performance. This containment design involves a tube-in-shell configuration where the PCM fills the annular space between concentric tubes with the heat transfer fluid (HTF) flowing inside the inner tube [16].

Fins are a widely adopted solution for overcoming the inherently low thermal conductivity of PCMs, which hinders heat transfer in LHTES systems [17]. Previous research has demonstrated fins to be an effective and practical enhancement technique. They augment heat transfer rates in LHTES designs by increasing the available heat exchange surface area and conductivity between the PCM and heat transfer fluid or solid structure. Notable early investigations include the work of Mat et al. [18], who evaluated the performance of internal and external fins integrated with concentric tubes. Their experimental results showed charging time reductions of 58% under constant fluid velocity circulation and 86% under constant inlet temperature conditions. This confirmed fins as a means to significantly accelerate the phase change process. Similarly, Rathod and Banerjee [19] examined the impact of annular fins installed in a vertical shell-and-tube exchanger. They reported melting and solidification time decreases of up to 25% and 44%, respectively, highlighting fins' beneficial effects on both thermal processes.

Comparative studies have provided further insights. One such analysis considered reductions in melting duration when using internal, internal-external, and external triangular fins versus longitudinal fins, reporting improvements of 11-15% [20]. Hendra et al. [21] also made contributions through their examination of paraffin-fat PCM charging behavior confined within a 16-tube shell-and-tube unit. Their findings led to the conclusion that heat conduction played a dominant role during charging, demonstrating the importance of conductive pathways provided by fins. Safari et al. [22] delved deeper into fin geometry influences, exploring variations in upper and lower fin length as well as shape configurations within concentric tube-shell designs. Their experimentation led to optimized melting enhancements. Pu et al. [23] performed numerical simulations comparing multiple radial PCM layers with gradient copper foam inserts. Their results determined single PCM arrangements performed most effectively, while negative foam gradients most efficiently transmitted heat. Additional insights were gained from studies focused on solar still designs. Suraparaju et al. [24] examined staggered-finned absorbers immersed within paraffin wax beds. The findings indicated that the solar still with a hollow-finned absorber, integrated into the energy storage system, outperformed other configurations and held promise for economically viable production of drinkable water.

Several studies have focused on experimenting new tubular designs within tube-based LHTES systems to improve heat transfer performance during charging and discharging cycles [25]. Assari et al. [26] experimentally evaluated a triplex tube exchanger with full width and half width sinusoidal inner tubes containing PCM. The full width sinusoidal tube exhibited shorter melting and solidification times compared to the half width tube when charging and discharging. Both sinusoidal designs significantly outperformed a straight tube in reducing melting time. Other works have explored incorporating various fin shapes directly onto tubes. PCM-filled systems incorporate circular, circumferential, longitudinal and rectangular fins, both internally and externally. Maciej et al. [27] experimentally analyzed tube bundles within a shell-and-tube heat exchanger using in-line and staggered configurations at different pitches. The in-line arrangement was optimal for melting while staggered improved solidification times. Additionally, Fadl et al. [28] developed and tested a horizontal multi-tube system using RT62HC PCM and water as HTF for building energy applications such as heating and hot water. Their aim was to analyze PCM temperature distribution, melting and solidification rates, and heat storage/release capacity. The parallel design met energy demands efficiently. Consistent results were obtained in other related studies [29-31] exploring features like enhanced internal tubes, integrated fin designs, tube bundle layouts, and integrated building thermal storage performance, demonstrating the continued efforts to improve tube-based LHTES performance through geometric modifications.

Several other studies have specifically focused on enhancing the PCM performance and effectiveness in building applications through the use of macro-encapsulation in bricks, wallboards, plates and storage tanks for active and passive implementations [32]. Given the importance of optimizing building envelope components, Laasri et al. [33] evaluated the impact of PCM incorporation in buildings and found a south-facing window orientation achieved up to 69.6% annual energy savings in a light-weight building in Morocco. More recently, topology optimization has emerged as a promising method for designing highly efficient fins with minimal trial-and-error in PCM units for building applications as demonstrated in works by Laasri et al. [34, 35]. However, few studies have specifically focused the integration of fins-enhanced shell-and-multi-tube LHTES units within the broader context of building energy management. Therefore, an opportunity remains to carry out a comprehensive and systematic optimization of fin-based geometric parameters within such an LHTES system.

In the present study, a systematic investigation of various geometric finned-tube parameters within the shell-and-multi-tube LHTES system is conducted to optimize heat transfer performance. For the baseline finned-tube cases, each tube was equipped with eight fins. Sixteen such finned tubes were used for the charging process, while another set of sixteen dedicated finned tubes were employed for discharging. Additionally, the study examined the charging process of the PCM in the presence of plain tubes without fins, in order to analyze the impact of fins through comparison. The aim was to clarify the effect of the dedicated discharge finned tubes, positioned strategically between the primary charging finned tubes, on enhancing heat communication within the PCM domain. Through comprehensive numerical modeling and analyses of key metrics such as heat storage rates, melting times, temperature distributions and fluid flow patterns, the impact of these differentiated fin designs on charging and discharging behaviors of high-enthalpy PCM (RT70HC) are demonstrated. The objective is to advance latent heat transfer efficiencies and identify optimized geometric mutations that can potentially improve the design of LHTES technologies for diverse thermal energy applications.

2. Problem description

This study explores the heat transfer optimization in a shell-and-multi-tube LHTES unit containing the high energy-density PCM (RT82) (Table 1). Figure 1 shows the complex three-dimensional arrangement and shape of the shell-and-multi-finned tube system being investigated. Part (a) provides a 3D view of the entire design setup. It consists of an outer cuboid shell containing multiple inner tubes arranged in a staggered layout. There are 16 finned tubes used for charging, shown in blue, and an equal number of 16 finned tubes dedicated for discharging, depicted in red. Each tube has 8 fins attached to it. The tubes contain a heat transfer fluid and are surrounded by a phase change material filling the shell space. Part (b) shows a two-dimensional cross-section of the domain shape. The staggered arrangement of the inner tubes with alternating rows for charging and discharging is clearly visible. The gaps between the tubes are filled with the PCM. The key feature is the strategic placement of discharge fins between the primary charging finned tube. This differentiated configuration enables comprehensive analysis of the discharging finned tube impact on optimizing heat distribution within the PCM domain.

A comparative analysis is performed to assess the mass of PCM in two different configurations. The finned tube configuration has a documented mass of 88 kg, while the plain tube equivalent has a slightly higher mass of 91.8 kg. The reason for prioritising the heat storage rate over solely analysing the melting time is to provide a more thorough and enlightening foundation for comparison. The findings indicate that the finned configuration has a heat storage capacity of 4.64 kWh, whereas the plain tube configuration has a heat storage capacity of 4.96 kWh. This intentional change in emphasis enables a more subtle comprehension of the complex heat retention patterns inside the system. Moreover, the practical implications of these findings are emphasized by the appropriateness of the storage unit dimensions for use in a compact building environment as illustrated in Figure 2. The figure highlights an integration of the developed PCM unit within a building-integrated photovoltaic-thermal (PVT) module. The thermal energy collected by the PVT module is transferred to the PCM-TES unit via a circulating heat transfer fluid, enabling efficient storage of thermal energy. The stored thermal energy in the PCM unit can be released and utilized for applications such as space heating as the thermal energy being directed to a heat pump for temperature upgrading. Additionally, the electricity generated by the PV cells can power the heat pump or meet other electrical demands. This integration offers advantages like energy storage, thermal load shifting, and demand management for building applications.

Table 1: Thermophysical properties of RT82 [36, 37].

Parameter (units)	**Value**
Density (kg/m^3)	825
Specific heat (J/kg.K)	2000
Thermal conductivity (W/m. K)	0.2
Viscosity (kg/m.s)	0.042
Thermal expansion coefficient (1/K)	0.00075
Solidous temperature (°C)	77
Liquidous temperature (°C)	82
Latent heat capacity (kJ/kg)	170

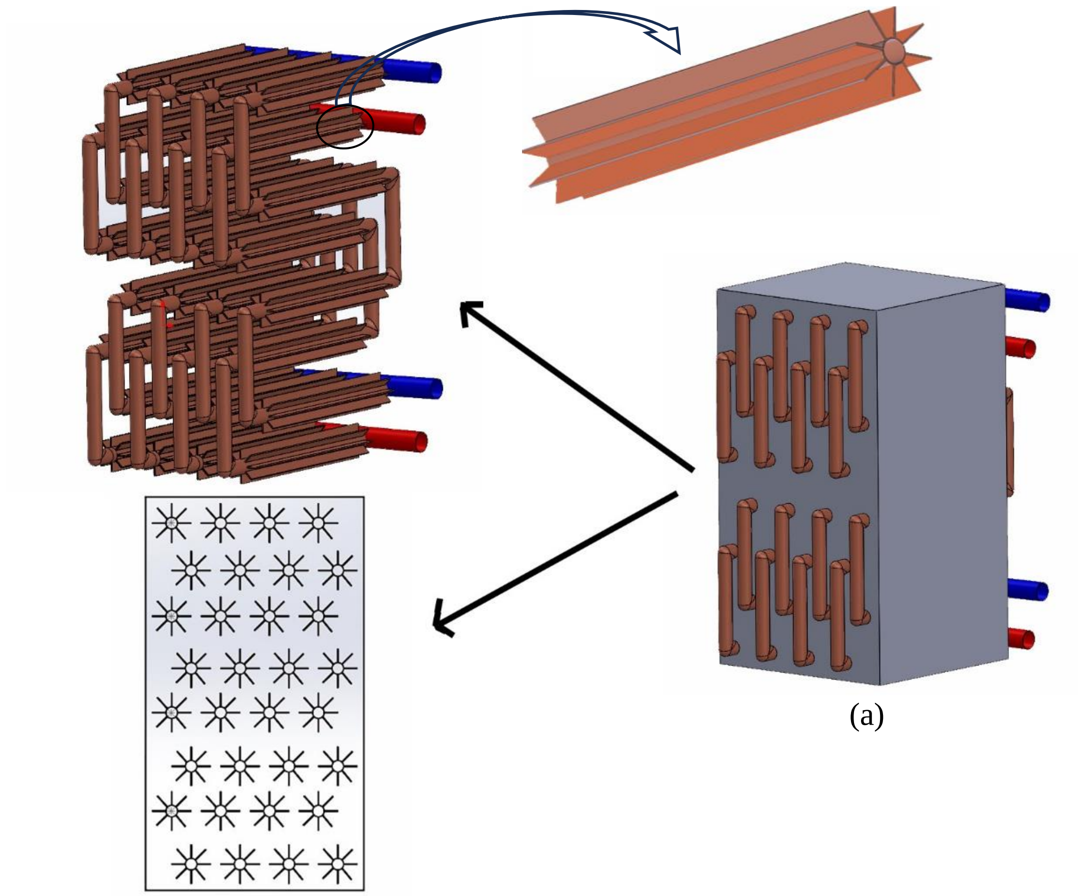

Figure 1. Schematic of the shell-and-multiple finned tube LHTES design: (a) three-dimensional and (b) internal representations and cross-section of the integrated charging and discharging tube network within the LHTES shell.

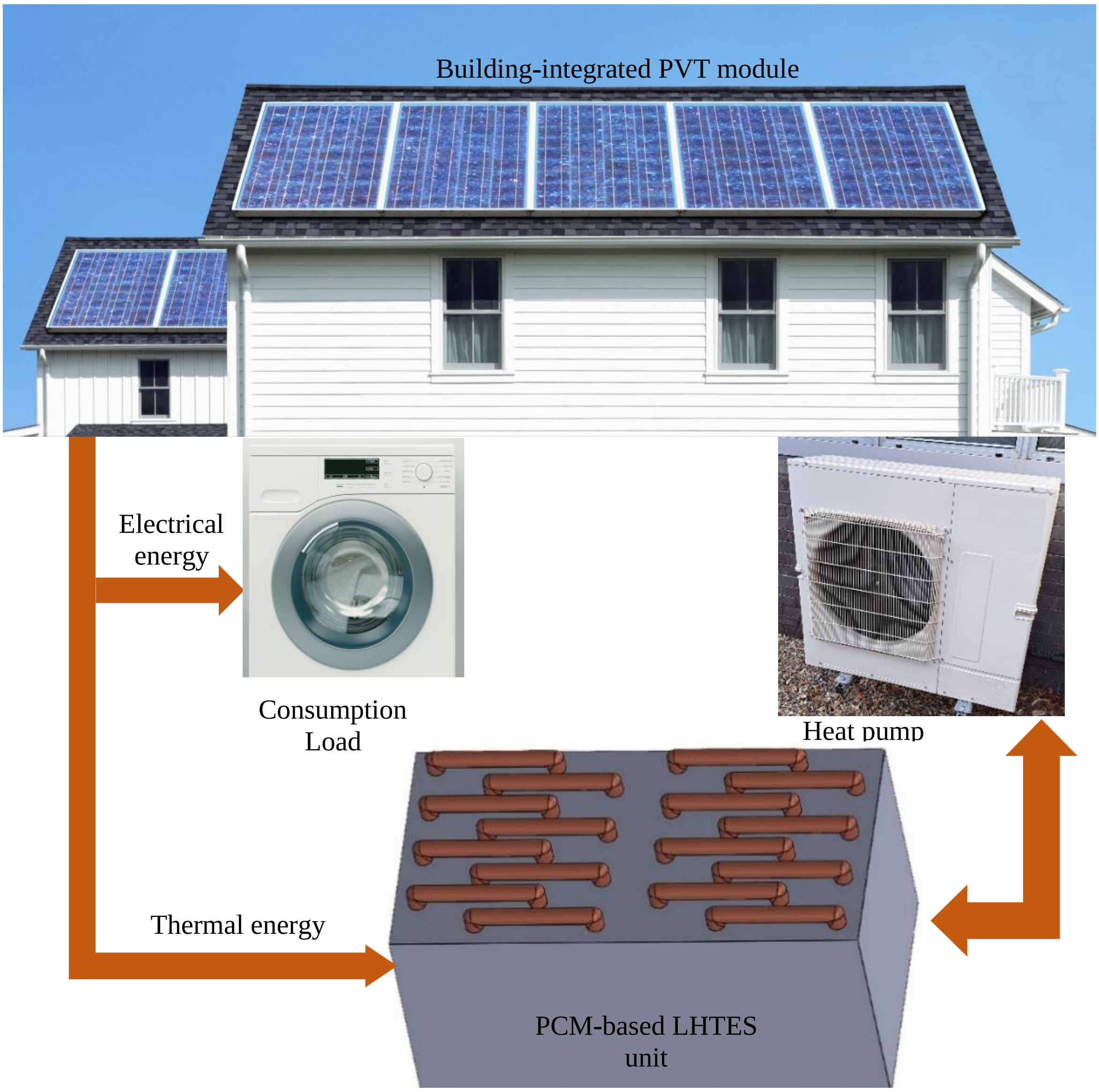

Figure 2. Schematic view for the integration of the LHTES unit with building-integrated PVT module for load shifting and energy management in buildings.

3. Mathematical formulation

3.1 Governing equations

Accurately simulating complex phase change dynamics of PCMs is crucial for optimizing LHTES design. The enthalpy-porosity modeling approach of Brent et al. [38, 39] provides an effective means for numerically replicating melting and solidification processes in Computational Fluid Dynamics (CFD)-based simulation [40]. This technique treats the multifaceted PCM zone as a homogeneous porous medium through introduction of the liquid fraction (λ) parameter. Each computational cell is assumed to maintain uniform porosity and λ

values during simulation. Density variations within the PCM are accounted for using the Boussinesq approximation, incorporating modifications to fluid properties based on temperature differences from a reference state. This enables consideration of buoyancy-driven natural convection induced by distinct liquid and solid phase densities [41]. Laminar, incompressible fluid flow with Newtonian rheology is presumed. Adiabatic conditions are imposed, neglecting viscous dissipation and external heat losses [42]. The conservation principles for continuity, momentum, and energy are applied under the given assumptions to formulate the following governing equations in simplified form.

$$\frac{\partial \rho}{\partial t} + \nabla . \rho \vec{V} = 0 \tag{1}$$

$$\rho \frac{\partial \vec{V}}{\partial t} + \rho\left(\vec{V}.\nabla\right)\vec{V} = -\nabla P + \mu\left(\nabla^2 \vec{V}\right) - \rho_{ref}\beta\left(T - T_{ref}\right)\vec{g} - \vec{S} \tag{2}$$

$$\frac{\rho C_p \partial T}{\partial t} + \nabla\left(\rho C_p \vec{V} T\right) = \nabla(k\nabla T) - S_L \tag{3}$$

The inclusion of the damping term ($\vec{S}$) in the momentum equation is due to the impact of the phase transition event. This statement corresponds to the definition of the damping coefficient in the Darcy law, as indicated in reference [43].

$$\vec{S} = A_m \frac{(1-\lambda)^2}{\lambda^3 + 0.001}\vec{V} \tag{4}$$

The literature indicates that the constant A_m for the mushy region is about 10^5, as documented in references [18, 44, 45]. The energy equation incorporates a source component to accurately consider the influence of latent heat and phase transition phenomena. The term encompasses the liquid portion of the PCM, represented as λ, as demonstrated in reference [46].

$$\lambda = \frac{\Delta H}{L_f} = \left\{\begin{array}{ll} 0 & if\ \ T < T_{Solidus} \\ 1 & if\ \ T > T_{Liquidus} \\ \dfrac{T - T_{Solidus}}{T_{Liquidus} - T_{Solidus}} & if\ \ T_{Solidus} \le T \le T_{Liquidus} \end{array}\right\} \tag{5}$$

The source term S_L in the energy expression is obtained as follows:

$$S_L = \frac{\rho \partial \lambda L_f}{\partial t} + \rho\nabla\left(\vec{V}\lambda L_f\right) \tag{6}$$

The rate at which energy is accumulated during the process of charging is subsequently defined as:

$$\dot{E}_T = \frac{E_e - E_i}{t_m} \tag{7}$$

The variable t_m represents the duration of the melting phase. E_e and E_i denote the overall energy of the phase change material at the conclusion and commencement of the melting process, respectively. The variable E represents the total energy content of the PCM, which includes both the sensible heat ($MC_p dT$) and latent heat (ML_f) of the material. It is important to acknowledge here that the governing equations for the flow of the heat transfer fluid adhere to the conventional Navier-Stokes equations, which do not account for the impacts of phase transition. It is also worth noting that while the solidification and melting temperatures of the PCM are 69°C and 71°C, respectively, as indicated in Table 1, the phase change temperature was considered to be 70°C in the numerical simulation for computational efficiency and ease of analysis.

3.2 Initial and boundary conditions

Initially, the PCM is either in a solid or liquid state, depending on the phase changing mode in charge.

- For the melting (charge) mode:

$T = T_{int}$ = 70°C (solid PCM) (8)

- For the solidification (discharge) mode:

$T = T_{int}$ = 85°C (liquid PCM) (9)

The temperature of the fins and tube is set equal to the HTF inlet temperature for the respective charging or discharging mode.

- At the inner tube surface (Wall-PCM interface):

$T = T_{HTF}$ = 85°C (for charge mode) (10)

$T = T_{HTF}$ = 70°C (for discharge mode) (11)

- At the outer shell surface:

$q = 0$ (adiabatic boundary, no heat flux) (12)

4. Numerical solution and grid independence

ANSYS-FLUENT was used to solve the equations governing the heat exchange system and phase transition process. The SIMPLE technique facilitated the coupling of pressure and velocity, whereas the Green-Gauss cell-based method computed gradients of variables. The

QUICK differencing program resolved the momentum and energy equations, while the PRESTO system implemented pressure correction techniques. The under-relaxation factors for the pressure correction, flow rate components, liquid percent, and energy formula were set to 0.3, 0.3, 0.5, and 1, respectively. The convergence thresholds for the continuity, momentum, and energy equations were set at 10^{-4}, 10^{-4}, and 10^{-6}, respectively.

Prior to initiating simulations, an analysis was performed to determine grid independence and determine the appropriate time step size. An investigation of mesh independence was conducted on the inline-finned design with a consistent arrangement of fins. The investigation included altering the diameters of individual cells to 1, 2, and 3 mm, as well as adjusting the time step sizes to 0.1, 0.2, and 0.4 s. The results exhibited consistent outcomes across all mesh dimensions. Consequently, a mesh size of 3 mm was chosen for further investigation due to its reduced cell count, as depicted in Figure 3(a). The analysis revealed that modifying the time step sizes (0.1, 0.2, and 0.4 s) for the chosen grid had no impact on the simulation time or the overall results, as shown in Figure 3(b). After careful consideration, a time step size of 0.4 s was ultimately selected.

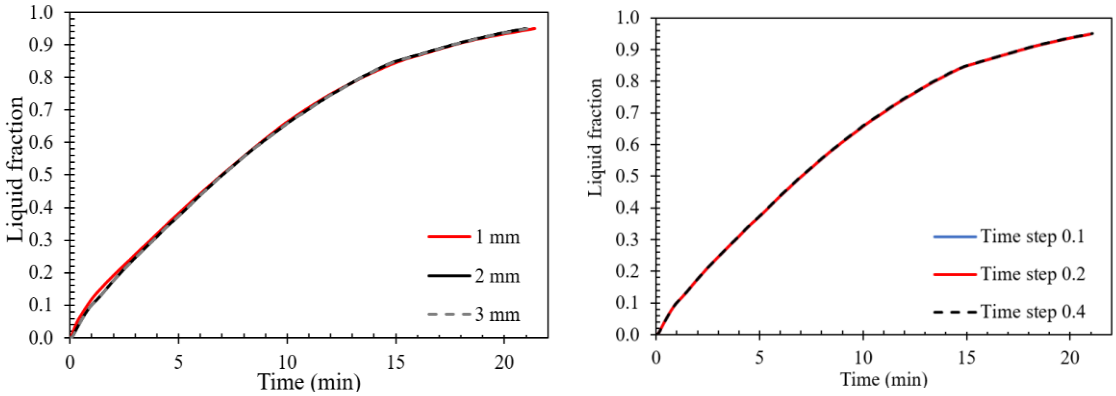

(a) (b)

Figure 3. Assessment of numerical solution accuracy for liquid fraction analysis using different (a) grid sizes and (b) time steps.

5. Numerical model validation

The numerical model was validated through a comparison with experimental data obtained from Al-Abidi et al. [47] to establish confidence in the accuracy of the heat transport and phase change physics represented by the developed numerical model. In their work, Al-Abidi et al. [47] investigated the melting and solidification behavior of PCM (RT82) in a concentric tube heat exchanger with radial fins. The geometrical model was set up to match the heat exchanger dimensions reported in [47], consisting of an inner tube of 25 mm radius, a middle annular region filled with a 50-mm thick layer of PCM, and an outer tube of 100 mm inner radius. Eight radial copper fins of 1 mm thickness extended at 45° intervals from the inner and middle tube surfaces into the annular PCM region. For melting validation, the inner and middle tube surface temperature was fixed at 90°C, while the outer tube and adiabatic outer surfaces were set as insulated boundaries. The initial PCM temperature was uniformly set at 30°C. For solidification validation, the tube surfaces were fixed at 30°C, while the initial PCM temperature was assigned as 90°C. The comparison of predicted melting and solidification temperatures versus experimental data from Al-Abidi et al. [47], as illustrated in Figure 4, showed good agreement, with maximum deviations of less than 1.5°C. This validates the numerical model's ability to accurately simulate heat transfer and phase change behavior in the tube heat exchanger configuration. Moreover, the model precisely predicts subtle physical phenomena, such as the melting plateau occurring at the moment of phase changeover. The strong correlation seen between quantitative temperature measurements and numerical predictions provides compelling evidence that the proposed numerical model can accurately replicate the expected heat transfer dynamics and phase shift behaviors in the examined latent heat storage system design.

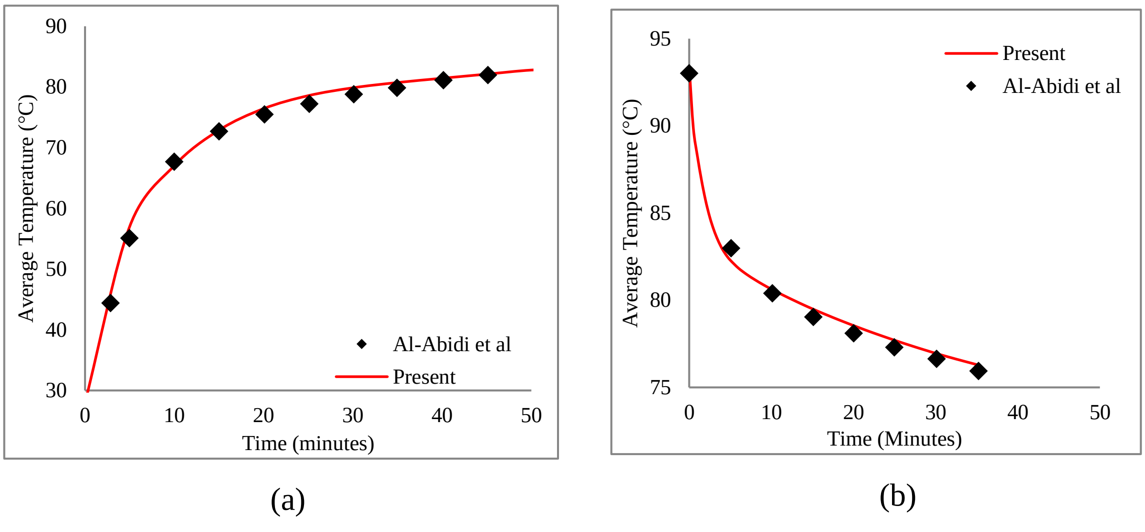

Figure 4. Model benchmarks during (a) the melting mode and (b) the solidification mode using the experimental findings of Al-Abidi et al. [47].

6. Results and discussion

This study investigated a shell-and-multiple-finned tube system utilizing RT70HC as PCM, which possesses a high latent heat of 240 kJ/kg. For the finned cases, each tube was equipped with eight fins. Additionally, 16 finned tubes were used for each charging and discharging process. The study also examined the charging process of the PCM in the presence of plain tubes (without fins) to analyze the impact of fins in the comparison. The aim was to assess the effect of discharging finned tube on enhancing heat transmission within the PCM between the charging finned tube.

6.1 Charging process dynamics

Figure 5 shows the liquid fraction of the PCM during the charging process over 10 hours for the plain tube case without fins. In the first 30 minutes, buoyancy-driven natural convection occurs as the higher density solid PCM contacts the tube wall, causing molten PCM with lower density to accumulate above due to temperature gradients inducing density variations governed by the Boussinesq approximation. Between 1-3 hours, continued absorption of thermal energy from the HTF flowing inside the tube via single-phase heat transfer raises the PCM temperature until it reaches the phase transition point, resulting in an increase in melted PCM volume that combines into a consistent front while vertically expanding the liquid domain through laminar flow modeled using the Navier-Stokes equations. By the 6-hour mark, all regions except the small domain near the shell wall in contact with the adiabatic boundary have transitioned from solid to liquid state as the solid-liquid interface evolves non-uniformly over time. After 10 hours, temperature stratification forms with the upper portion reaching thermal equilibrium at the HTF temperature more rapidly than the lower section undergoing two-phase heat transfer, which relies on slower dissipation of heat from the tubes into the surrounding PCM using the enthalpy method to accurately model the complex phase change dynamics in the plain tube configuration.

Figure 6 shows the temperature distribution in the PCM domain during the 10-hour charging process. In the initial 30 minutes, the temperature rises rapidly near the tube walls as heat is conducted from the hot HTF inside the tubes. This creates temperature gradients that drive natural convection currents, seen by the upward flow of warmer, less dense molten PCM. Between 1-3 hours, the absorbed thermal energy continues raising the PCM temperature until reaching the phase transition point. This results in an expanding front of melted PCM as the solid-liquid interface advances upwards through laminar flow. By 6 hours, nearly all regions except for a small domain near the adiabatic shell wall have undergone phase change, indicative of the ongoing solid-liquid transition. At 8 hours, the domain splits into three areas - the yellow portion of the PCM's top rises in temperature due to accumulation of warm molten PCM; the PCM below the tubes is either melted or transitioning from solid to liquid at lower temperatures; the third area contains still-solid PCM near the container wall. This division emphasizes how the dynamic charging processes shape regional temperature variations. By the end of the 10-hour period, the domain further stratifies into four sections. The warmest molten PCM remains at the top while the middle portion remains cooler due to heat dissipating from the tubes. This is why transitioning temperatures are seen lower down while the coolest still-solid PCM lies by the wall.

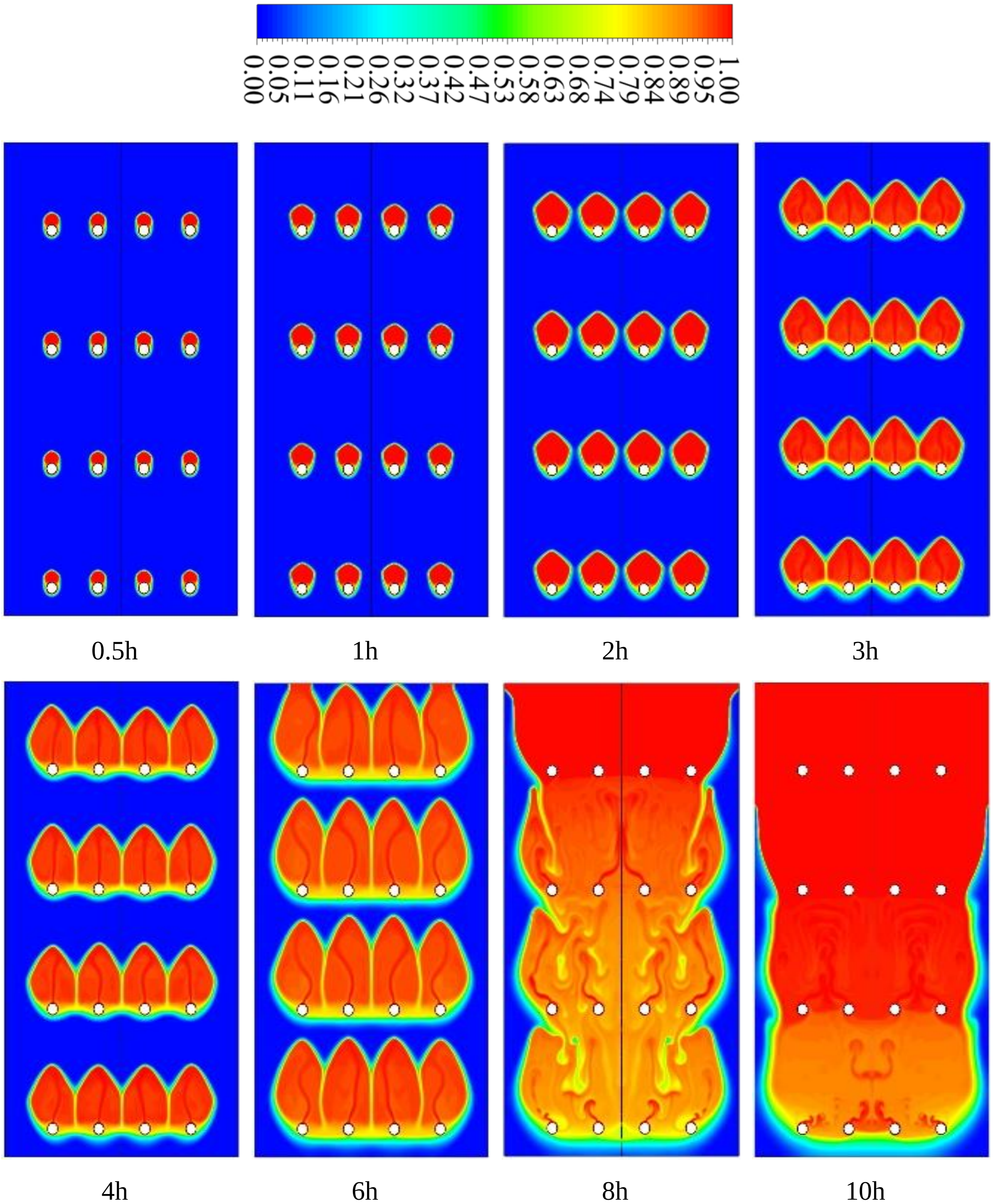

Figure 5. Time-dependent visualization of PCM liquid fraction from initial melting up to 10 hours for the case of the plain tubes.

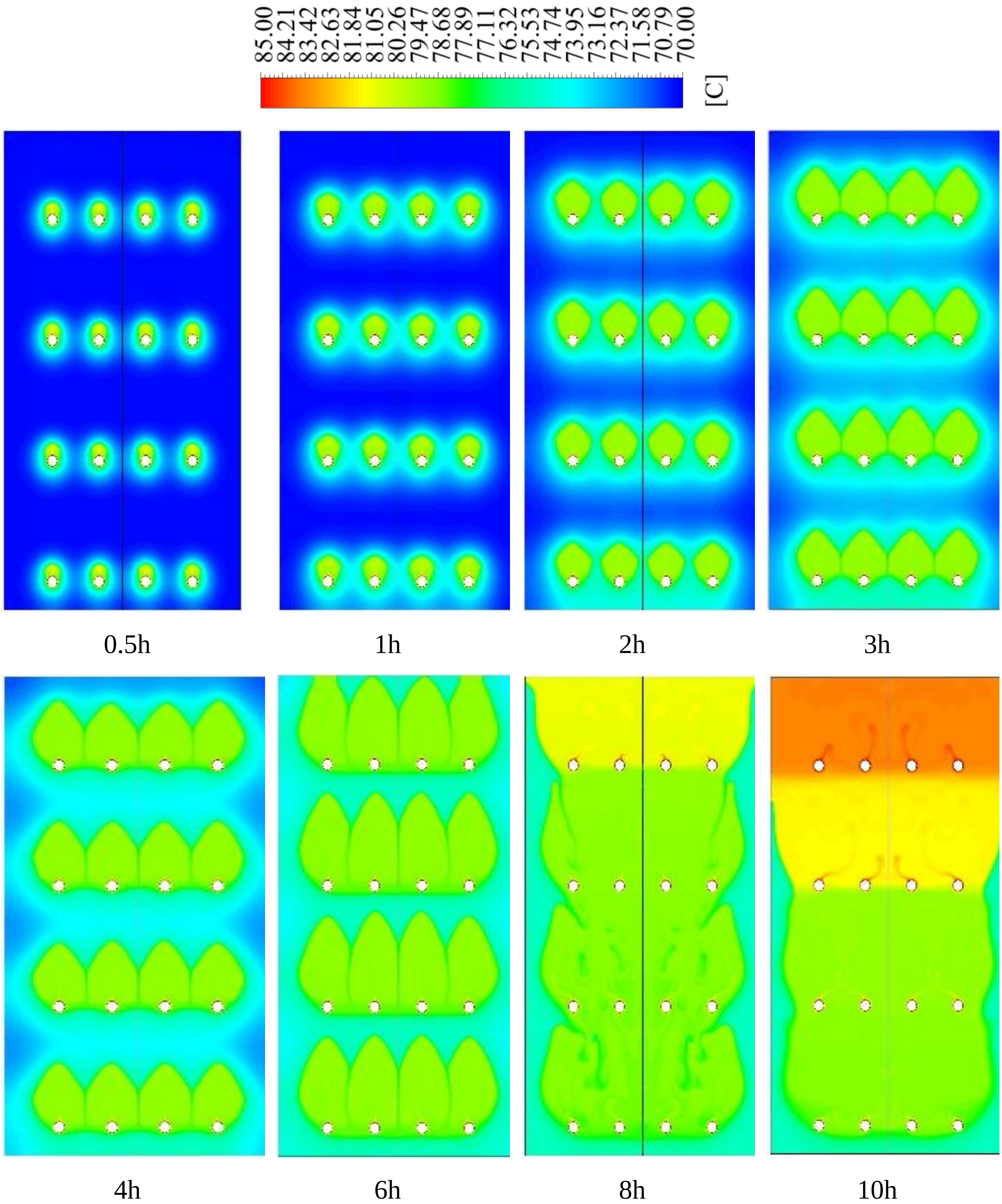

Figure 6: Time-dependent visualization of PCM temperature from initial melting up to 10 hours for the case of the plain tubes.

Figure 7 shows the liquid fraction evolution of the PCM at different time intervals during the heat exchanging process up to 4 hours for the case of the finned tubes. Within the first 10 minutes, a significant portion of the PCM surrounding the tubes and fins melts, as seen by the increase in the liquid fraction. This indicates that heat transfer occurs more rapidly via the highly conductive fins compared to the PCM. Between 10-30 minutes, the liquid fraction continues increasing as more PCM absorbs heat and melts. The fins facilitate efficient conduction of heat from the hot HTF, accelerating the melting of adjacent PCM. By 1 hour, over 50% of the PCM has melted. The close spacing between hot tubes enhances heat transfer between tubes via convection currents in the molten PCM and conduction through the fins. Between 1-2 hours, the liquid fraction keeps rising steadily as the melting front propagates further. By 3 hours, 93% of the PCM turned liquid, leaving only some areas above the cold tubes remaining solid. In the subsequent hour, the liquid fraction rises further to over 99.5% as the last remaining parts of solid PCM absorb sufficient heat energy to almost completely melt.

Figure 8 shows the temperature distribution of the PCM at different time intervals during the 4-hour heat exchanging process for the case of the finned tubes. Within the first 10 minutes, the temperature rises noticeably near the tubes and fins as heat is effectively conducted from the hot HTF. This creates temperature gradients driving natural convection. Between 10-30 minutes, absorbed heat continues raising the temperature across more of the PCM domain until regions around the tubes surpass the melting point. After reaching 1 hour, significant temperature stratification is seen with the hottest regions concentrated around the fins and tubes. This establishes a thermal gradient facilitating natural convection currents in the PCM. Between 1-2 hours, conduction and convection enhances broader temperature rises, with melting beginning around the tubes. At 4 hours, thermal equilibrium is achieved with a nearly uniform temperature profile, indicating efficient heat distribution across the system. The temperatures initially increase most rapidly around the fins and tubes due to their higher thermal conductivity. Over time, natural convection and conduction spreads thermal energy more uniformly through the PCM domain. The formed distribution emphasizes on how fins enhance heat transfer rates by raising temperatures much more quickly compared to designs without fins.

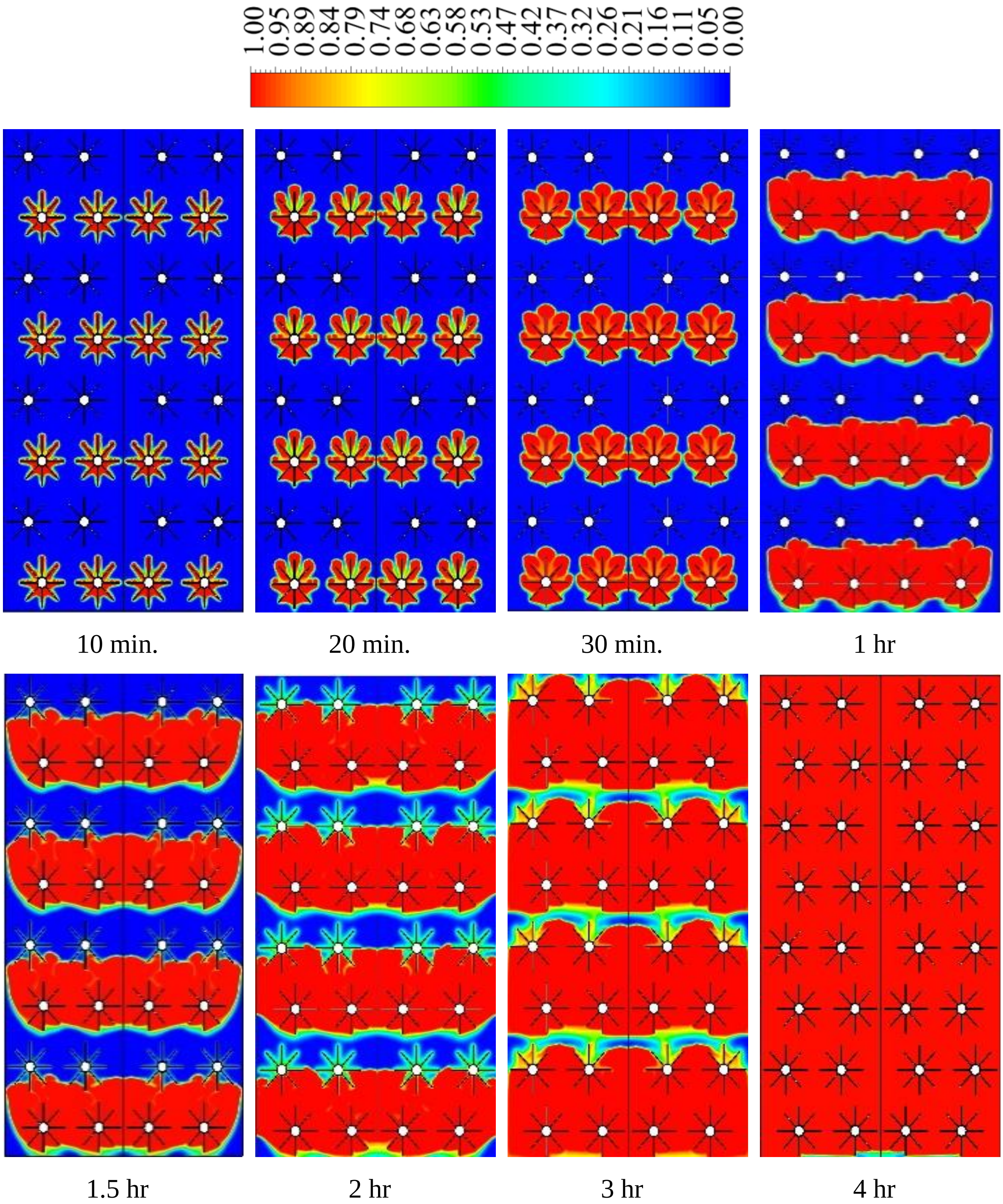

Figure 7. Time-dependent visualization of PCM liquid fraction from initial melting up to 4 hours for the case of the finned tubes.

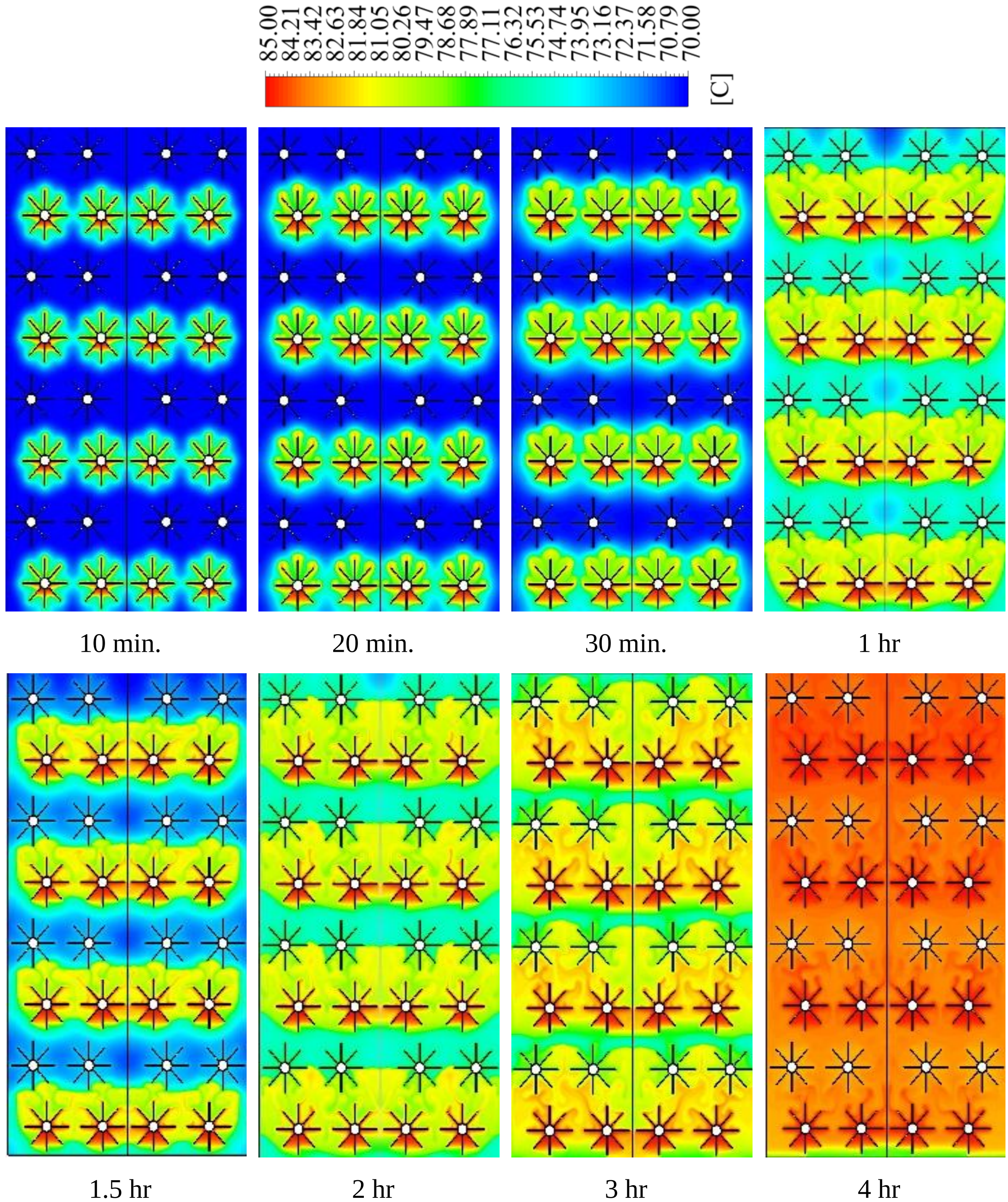

Figure 8. Time-dependent visualization of PCM temperature from initial melting up to 4 hours for the case of the finned tubes.

Figure 9 shows the velocity distribution of the PCM at different time intervals up to 4 hours during the charging process. Initially at 0.5 hours, lower velocity convection currents are observed in the liquid PCM regions near the tubes and fins. This is due to limited buoyancy forces induced by temperature gradients in the early stages of heating. As time progresses to 1 hour, the velocity magnitude increases slightly as the system absorbs more heat, evidenced by the expanding high velocity red regions. At 2 hours, the velocity continues increasing across most of the domain as the PCM temperature becomes more uniform during the ongoing phase change process. By 4 hours, the PCM velocity has significantly improved further, with higher velocities seen throughout the unit. This trend of increasing velocity over time is attributed to the melting process which increases temperature differences in the PCM. Initially, small temperature gradients cause low natural convection currents, driving lower velocities. But as the PCM absorbs more heat, the temperatures gradually increases, increasing buoyancy forces as hotter, less dense PCM rise, which later promotes relatively higher velocities. By 4 hours, the PCM is nearing a completely molten state at high temperature distribution. This promotes further density variations that induce stronger natural convection, evidenced by the very high velocities. So, this velocity analysis provides insights into the complex fluid flow dynamics occurring as the PCM transitions from solid to liquid during charging.

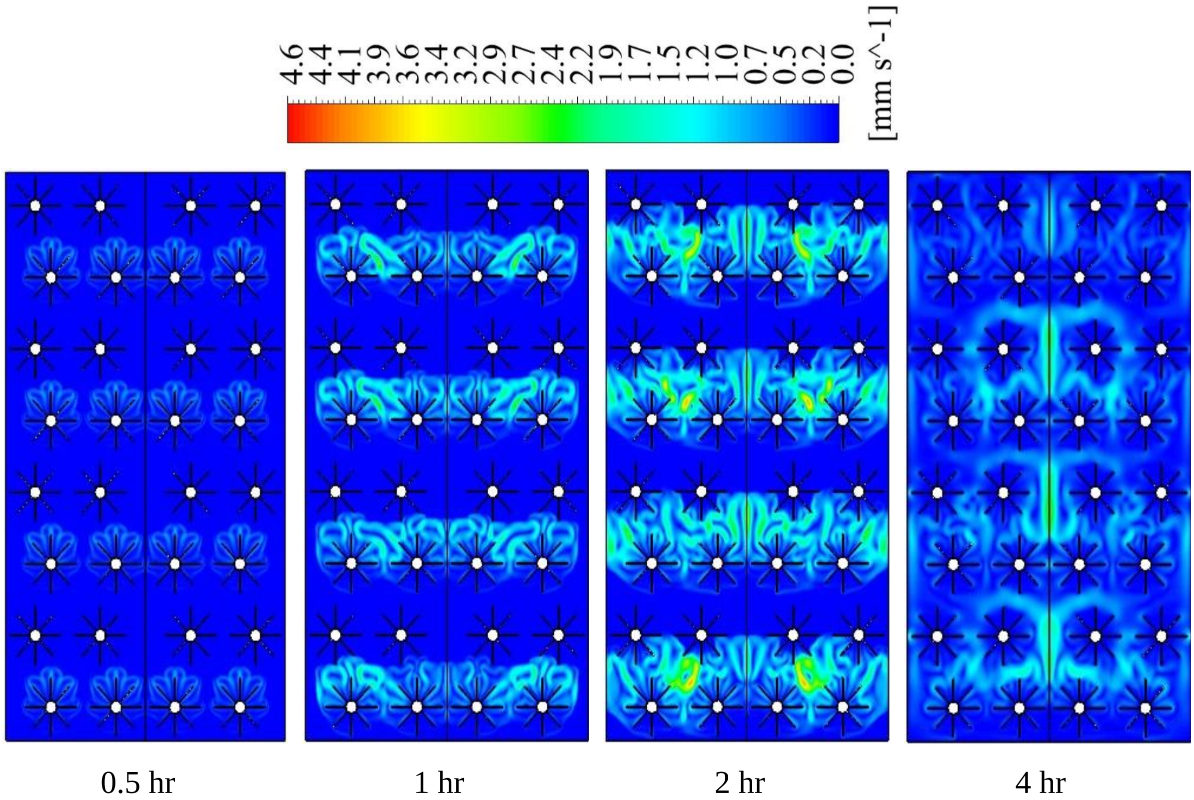

Figure 9. Time-dependent visualization of liquid PCM velocity from initial melting up to 4 hours for the case of the finned tubes.

Figure 10 shows the average liquid-fraction profiles which reveal that the finned tube configuration enables markedly faster melting of the PCM compared to the plain tube design without fins. Specifically, in the case of finned tube, the liquid fraction rises rapidly, reaching near complete melting after only 4 hours, while the liquid fraction in the case of plain tube increases slower, only attaining around 0.8 melted after 10 hours. Correspondingly, the finned tube heats the PCM to higher temperatures faster, as shown in Figure 11. It achieves 87°C after 3.5 hours versus the plain tube only reaching 86.6°C after 13.5 hours. This demonstrates the fins significantly improve heat transfer rates from the hot heat transfer fluid into the PCM due to increased surface area and conductivity. Consequently, the finned tube provides accelerated charging performance demonstrated by the much faster melting rate.

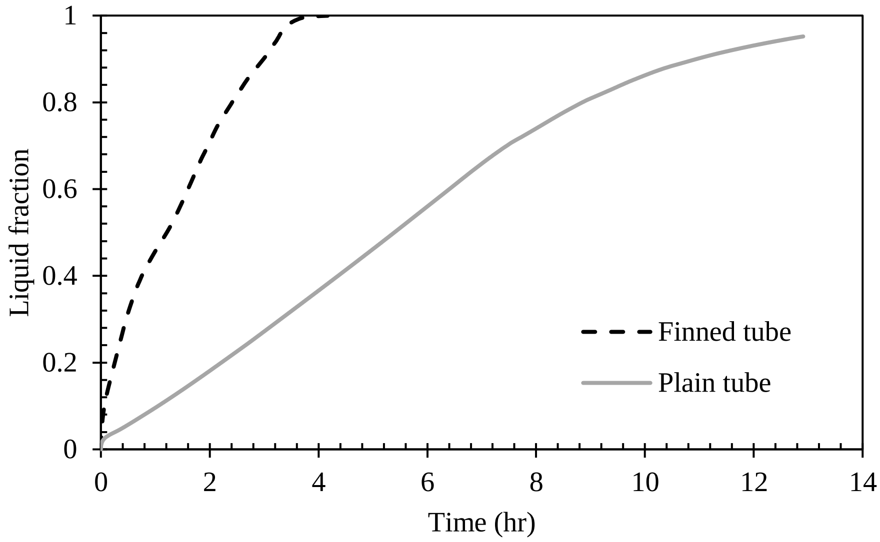

Figure 10. Time-varying profiles of PCM liquid fraction during charging process for cases of finned and plain tubes.

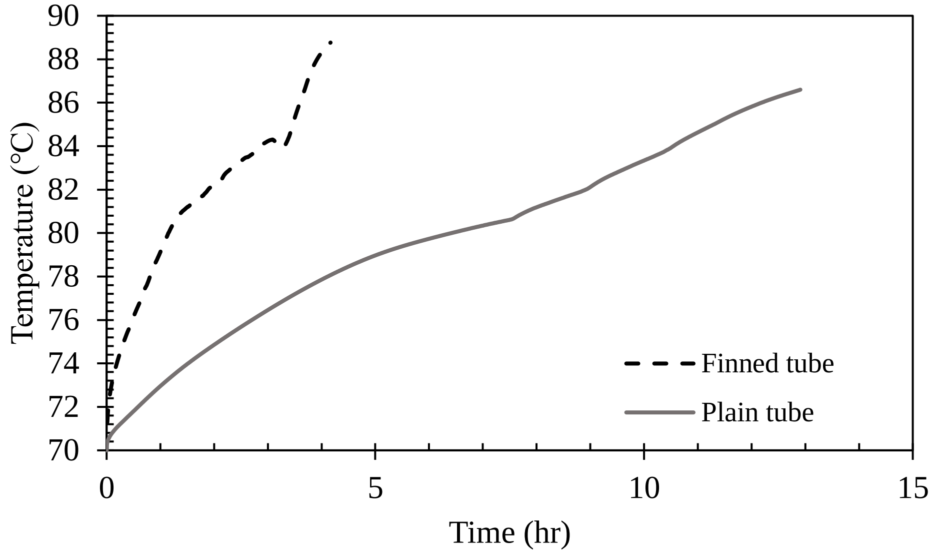

Figure 11. Time-varying profiles of PCM temperature during charging process for cases of finned and plain tubes.

Figure 12 compares the heat storage rate and melting time for the finned tube and plain tube configurations. The data reveals the finned tube has a significantly higher heat storage rate of 1421 W, compared to just 387 W for the plain tube. This equates to over a 268% increase in the heat storage rate enabled by the finned design. The higher heat storage rate stems from the fins increasing the heat transfer surface area in contact with the PCM. This allows more effective absorption of thermal energy from the hot HTF flowing inside the tubes during charging. Additionally, the fins provide supplementary heat conduction pathways to transport energy into the PCM, further improving the charging rate. This large disparity in heat storage rates highlights the substantial enhancement provided by the fins. Regarding melting time, the data shows the finned tube requires only 196 minutes to fully melt the PCM, whereas the plain tube needs 770 minutes to completely melt the PCM. This translates to the finned tube having a melting time about 61% shorter than the plain tube without fins. The reduced melting time for the finned configuration is a direct result of the higher heat storage rate enabled by the fins. Faster absorption of thermal energy leads to accelerated phase change from solid to liquid PCM. Therefore, the fins allow the melting process to complete much quicker, which offers obvious operational and economical benefits.

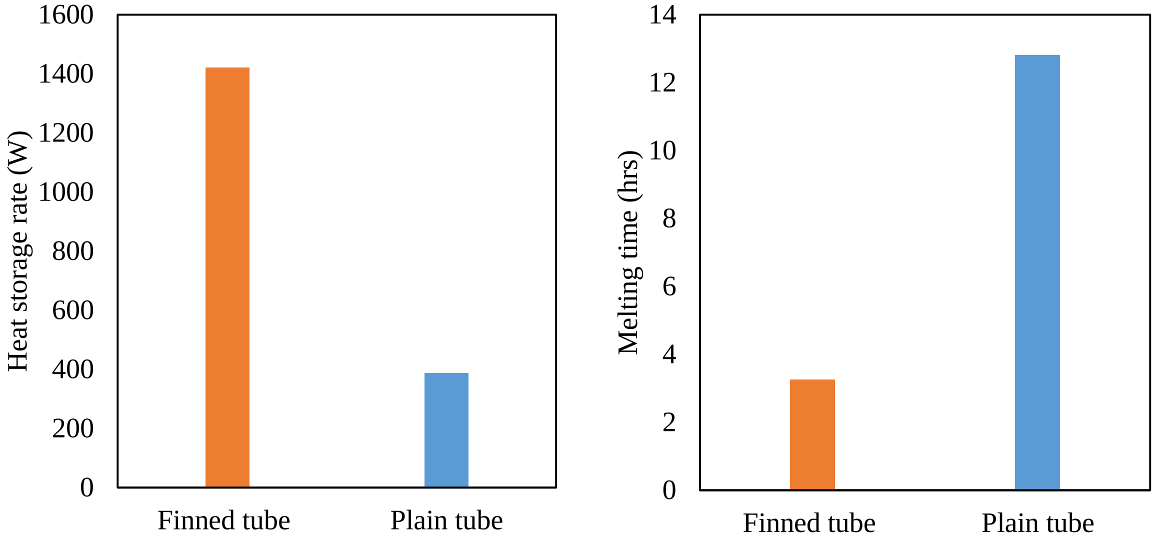

(a) (b)

Figure 12. Comparison of (a) heat storage rate and (b) melting time for finned and plain tube configurations.

6.2 Discharging process dynamics

Figures 13 and 14 show the liquid fraction and temperature evolution contours of the PCM during the discharging process over a period of 16 hours for the finned tube configuration. In the first 20 minutes, the liquid fraction remains at 1, indicating the PCM is still fully melted. Meanwhile, the temperature is stratified, with the hottest region concentrated around the fins and tubes which act as efficient heat conduction pathways. This creates thermal gradients in the PCM. After 1 hour, the liquid fraction near the cold tubes and fins begins dropping below 1 as those areas start solidifying first. Simultaneously, the temperature continues decreasing non-uniformly near the cold tubes and fins. This indicates the initiation of the solidification process in those regions. Between 2-4 hours, the solidified area expands outwards from the tubes and fins. The liquid fraction contours show the distinct solid-liquid interface propagating through the PCM domain. The temperature also decreases further during this time. By 8 hours, the solidified region has significantly grown, encompassing most of the area between the tubes. The liquid fraction plot indicates around 30-40% of the PCM remains melted. Meanwhile, the temperature has declined more uniformly, though stratification is still seen with warmer regions concentrated at the top. Overall, the data from the figures demonstrates that fins accelerate solidification by acting as thermal conductive pathways, enabling faster heat extraction from the PCM. This is evidenced by the thermal stratification which remains present even after 8 hours due to the differentiated cooling effects of the tubes and fins. This emphasizes the complex thermal interactions at play. After 16 hours, the system is moving closer to a thermally stable condition as evidenced by the creation of a coherent solid mass around the cold tubes.

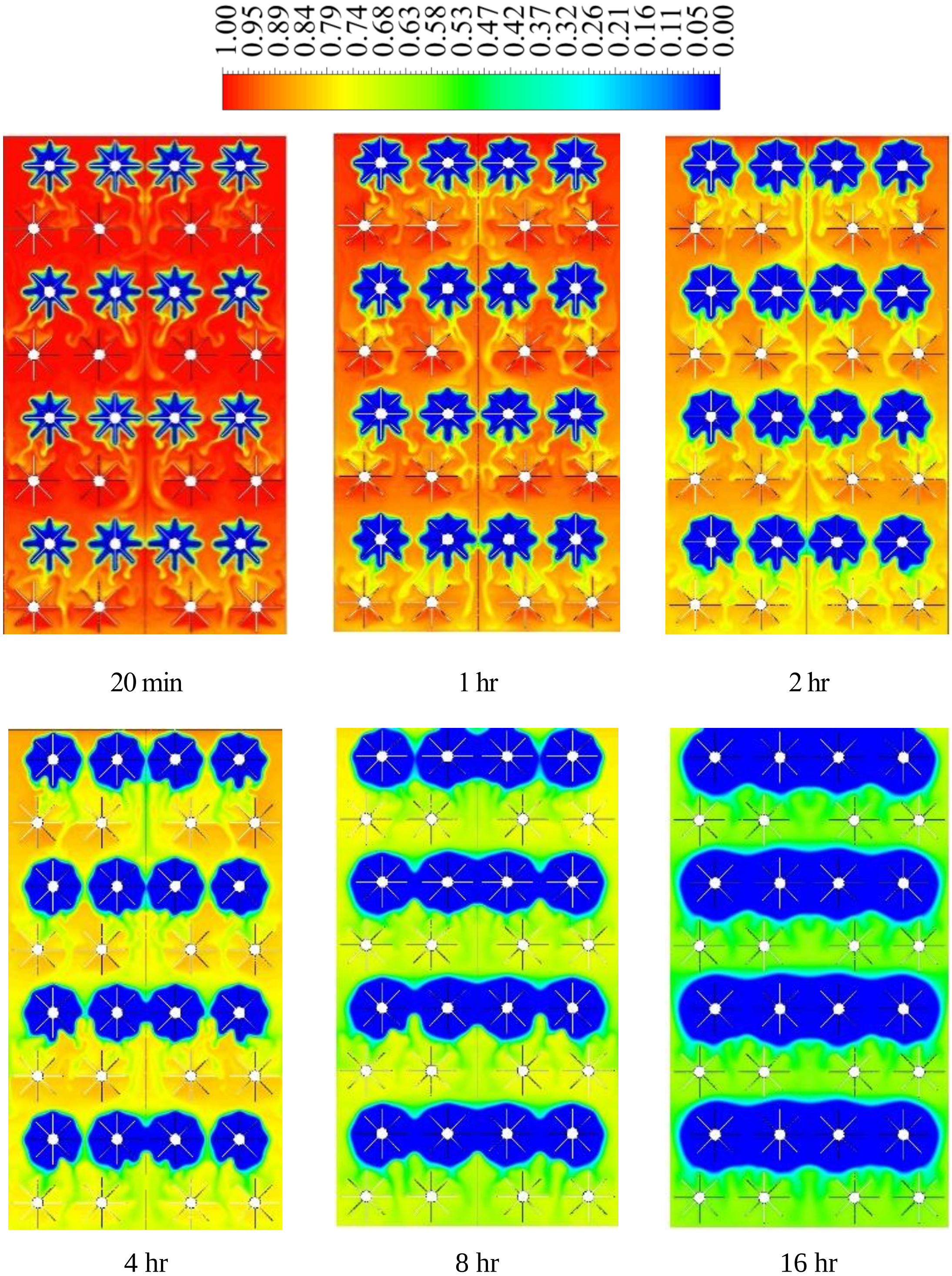

Figure 13. Time-dependent visualization of PCM liquid fraction from initial solidification to near-completion.

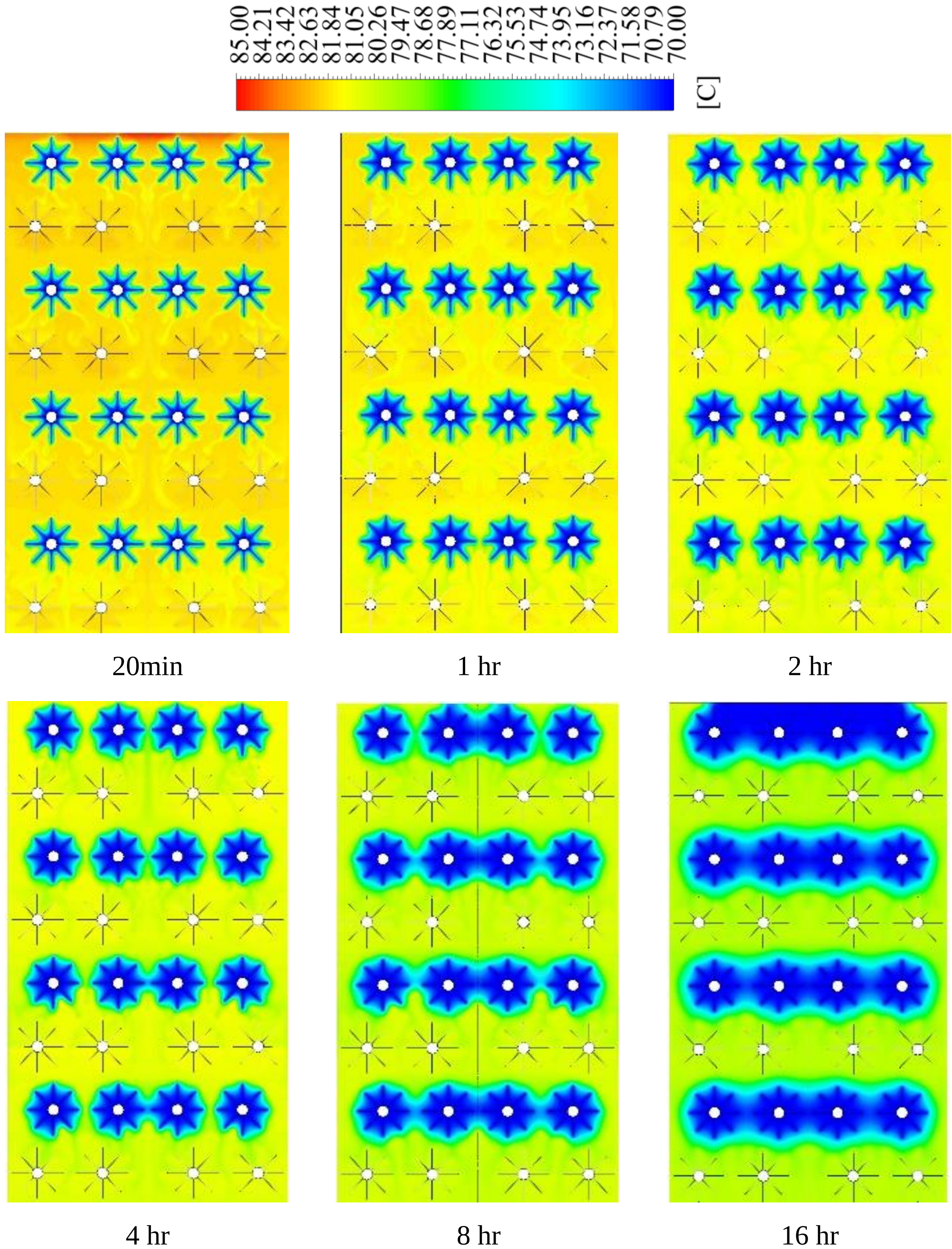

Figure 14. Time-dependent visualization of PCM temperature from initial solidification to near-completion.

Figure 15 shows the velocity magnitude contours of the PCM during the solidification process over 4 hours for the finned tube configuration. At 20 mins, distinct high velocity convection currents are seen between the tubes and fins. This is due to natural convection induced by thermal gradients created as the PCM solidifies around the cold tubes, extracting heat. After 1 hour, the velocity magnitude has decreased slightly as the ongoing solidification around the tubes reduces temperature differences in the PCM, lowering buoyancy forces driving natural convection. Between 2-4 hours, the velocity continues declining progressively across the domain as solidification advances, evidenced by the reducing size of high velocity red regions. By 4 hours, the velocity has slowed significantly, with very minimal residual velocities remaining. This indicates solidification is nearing completion, supported by minimal liquid PCM left. The initial high velocities are due to large thermal gradients causing natural convection currents in the molten PCM. As solidification occurs via heat extraction by the tubes, the temperature differences decrease, reducing buoyancy forces and progressively lowering velocities. The minimal velocities at 4 hours signify the nearly complete solid phase with negligible fluid motion. The velocity data provides insights into the complex convection dynamics occurring during solidification. It demonstrates the thermal gradients early on induce faster velocities that decline over time as temperatures equalize and the PCM solidifies.

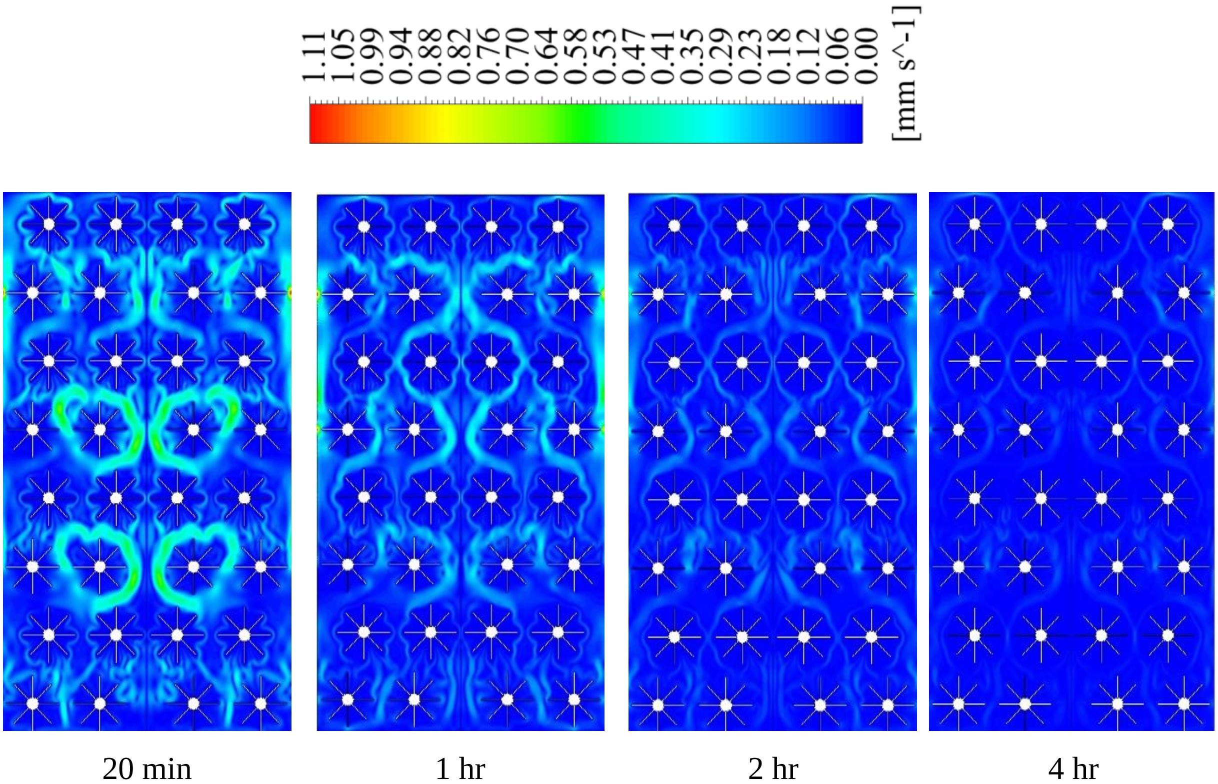

Figure 15: Time-evolution of the liquid PCM velocity from initial solidification to near-completion.

Figure 16 shows the liquid fraction and discharge rate profiles during the 20-hour discharging/solidification process for the finned tube configuration. Initially, the liquid fraction starts at 1, indicating the PCM is fully melted. Correspondingly, the discharge rate is at its maximum of around 2000 W. Over the first 4 hours, the liquid fraction declines rapidly to around 0.6 as significant solidification occurs. This is enabled by large temperature differences between the warm PCM and the cold HTF, allowing high heat extraction rates. Between 4-12 hours, the liquid fraction decreases at a slower, more gradual rate, reaching approximately 0.2 after 12 hours. This indicates solidification is progressing but is slowed as the temperature gradient reduces. After 12 hours, the liquid fraction continues decreasing at an even slower rate. Simultaneously, the discharge rate shows a corresponding gradual reduction over time. By 20 hours, around 10-15% liquid PCM remains. The discharge rate has declined significantly to about 100 W. The reducing liquid fraction and discharge rate aligns with expectations as temperature differences decrease between the PCM and HTF over time, lowering the heat transfer rate. The rapid early decline gives way to more gradual decreases in both liquid fraction and discharge rate. This represents the slowed solidification process as the system approaches thermal equilibrium.

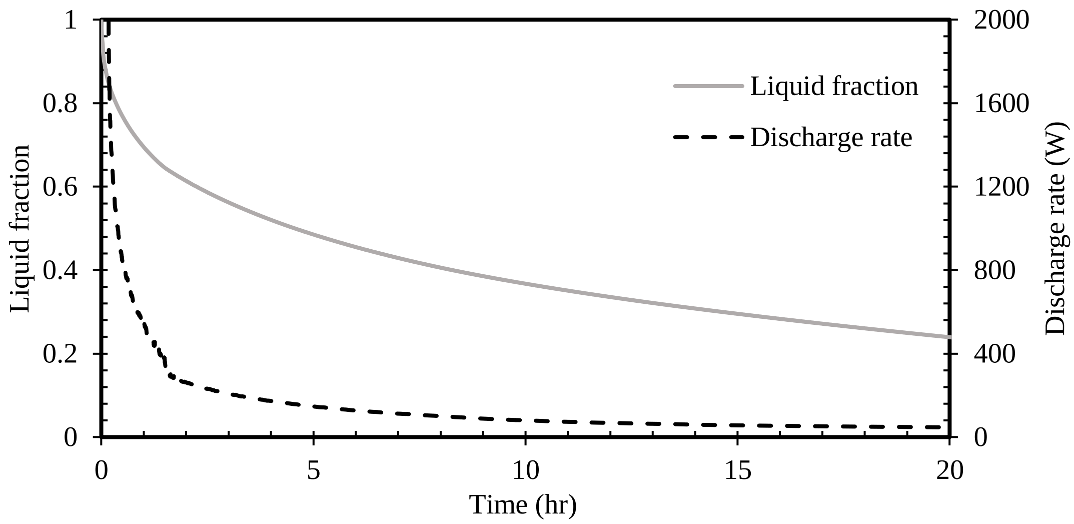

Figure 16. Time-varying profiles of liquid fraction and discharge rate during discharging process.

Figure 17 shows the temperature profiles of the solidification fins, melting fins, and average PCM during the 20-hour discharging/solidification process. The solidification fins remain fixed at 70°C throughout the process. This is due to their direct contact with the cold HTF circulating through the tubes. In contrast, the melting fins maintain a consistently high temperature of around 90°C. This is enabled by the hot HTF flowing in the separate tubes used for charging. Initially, the average PCM temperature starts at 90°C, representing its fully melted state containing sensible and latent heat. Over the first 4 hours, the PCM temperature decreases rapidly as heat is extracted via solidification around the cold tubes and fins. From 4-12 hours, the decline in PCM temperature slows as solidification rate decreases with reducing temperature differences. By 20 hours, the average PCM temperature has dropped to 76°C, indicating significant heat removal. The fixed solidification fin temperature demonstrates their role in providing a constant cold source to drive heat extraction for phase change. The steadily high melting fin temperature shows that separate tubes are used to maintain a hot HTF supply for charging. The reducing PCM temperature aligns with expectations as heat is dissipated to the cold HTF, leading to cooling and solidification. The temperature trends align with the liquid fraction and discharge rate profiles, emphasizing the consistent physical behavior during discharging.

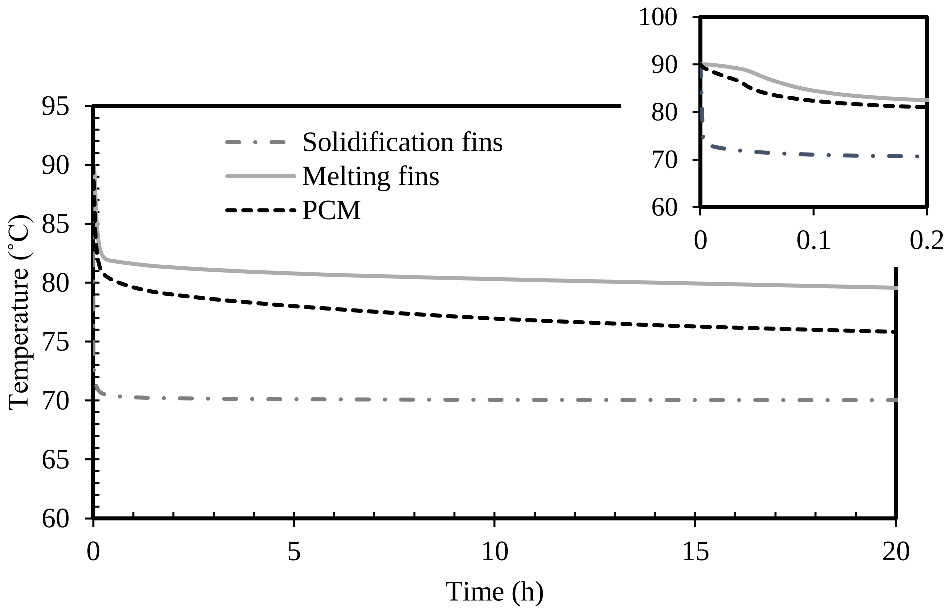

Figure 17. Temperature response of solidification fins, melting fins and PCM during discharging process. The inset displays the temperature profile in the first 12 minutes.

Figure 18 shows the discharge rate at different time intervals during the 20-hour heat exchange process. The discharge rate starts at a high value of around 2000 W in the initial stages. This high initial rate can be attributed to the large temperature difference between the fully liquid PCM and the cold HTF when discharging begins. In the first 5 hours, the discharge rate drops sharply from 2000 W to around 500 W. This sharp decline occurs because the temperature difference driving heat transfer decreases substantially as the PCM cools and begins to solidify around the cold tubes. Solidification extracts significant heat from the PCM, reducing its temperature. This in turn lowers the driving force for heat transfer to the cold HTF. Within 5-10 hours, the discharge rate continues to decline, but at a more gradual rate compared to the initial 5 hours, dropping to around 300 W. This gradual reduction indicates that the temperature differential is decreasing more gradually as the system starts to approach thermal equilibrium, with less heat remaining in the solidifying PCM to be transferred to the cold HTF. After 10 hours, the discharge rate tapers off slowly, reaching near-zero values by the 20 hour mark. The slow decline near the end suggests that the system has attained near-complete solidification with little remaining heat available to dissipate to the HTF. The declining trend of the discharge rate over time corresponds well with expectations, as solidification proceeds and reduces the temperature differences that drive heat extraction via the cold HTF. It closely mirrors the decrease in liquid fraction and average PCM temperature seen in other figures.

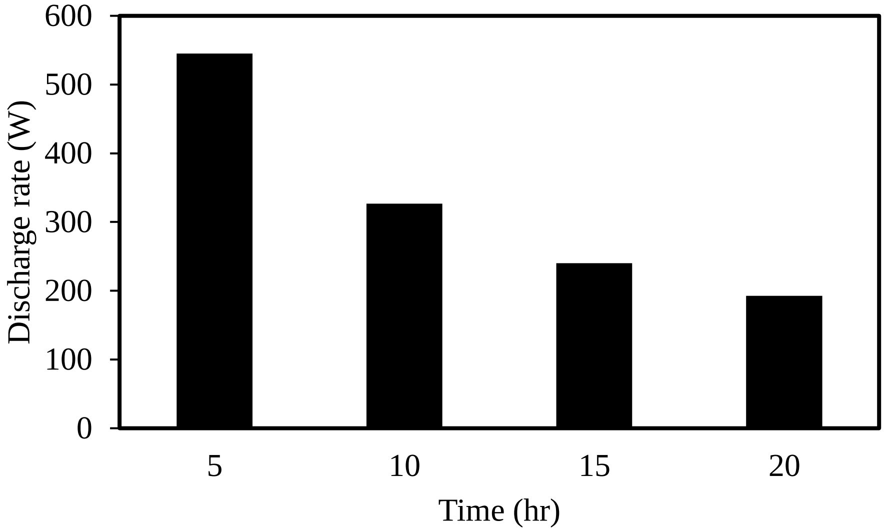

Figure 18. Progressive reduction of heat discharge rate over time during the discharging process

7. Conclusion

The present study performs comprehensive CFD analysis into the heat exchange behavior and solid-liquid phase change kinetics occurring in shell-and-multi-tube latent thermal energy storage systems. The staggered placement of 16 finned tubes for charging and 16 dedicated finned tubes for discharging enabled strategic examination of the complex melting and solidification phenomena. The following main conclusions could be drawn from this study:

1. The suggested finned tube configuration increased the charging rate by 268% from 387W to 1421W and accelerated the melting time by 61% from 770 mins to 196 mins compared to plain tubes without fins. This aligns with a heat absorption enhancement from 4.96 kWh to 4.64 kWh in the lower-mass 88 kg finned case.
2. Detailed 10-hour melting analysis revealed that, while initial conduction drives heating near fins, gradually strengthening buoyancy-induced convection currents distribute absorbed thermal energy deeper into the PCM domain, leading to stratification and eventual thermal equilibrium.
3. The present simulations accurately captured the coherent physical responses during the 16-hour solidification process, with the discharge rate decaying exponentially from 2000W down to 100W in tandem with the liquid fraction reduction from 1.0 to 0.1, as average temperatures dropped from 90°C to 76°C.
4. The constant 70°C and 90°C temperatures maintained by the fixed solidification and separate melting fins accentuated the role of differentiated fluid circuits in facilitating symmetric charge-discharge cycling.
5. The quantitative and qualitative results and analyses provided an important insight into the enhancement of heat transfer rates by over 268% through purposeful incorporation of bio-inspired fins. This sets the stage for multi-objective optimization of unconventional fin shapes targeting compact 100kWh-class shell-and-tube phase change storage systems tailored to renewable energy technologies.

While this study demonstrated significant improvements in PCM performance through optimized fin configurations in a shell-and-multi-tube LHTES unit, there remain opportunities for further advancements. Future research has the potential to surpass the present limitations by including additional high energy-density PCMs and/or diverse geometric configurations of fin arrays. Furthermore, future research could explore the integration of model predictive control (MPC) systems [48] to optimize energy management in buildings, leveraging the dynamic thermal storage capabilities of PCM. Additionally, investigating alternative fin distributions, including non-uniform or bio-inspired designs, could enhance the heat transfer efficiency and adaptability of the LHTES units under varying operational conditions. Finally, utilizing different machine learning algorithms such as Physics Informed Neural Network (PINN) [49, 50] towards optimization of the fin design could be utilized.

References

[1] H. Togun, H.S. Sultan, H.I. Mohammed, A.M. Sadeq, N. Biswas, H.A. Hasan, R.Z. Homod, A.H. Abdulkadhim, Z.M. Yaseen, P. Talebizadehsardari, A critical review on phase change materials (PCM) based heat exchanger: Different hybrid techniques for the enhancement, Journal of Energy Storage 79 (2024) 109840.
[2] H.M. Taqi Al-Najjar, J.M. Mahdi, T. Alsharifi, R.Z. Homod, P. Talebizadehsardari, A. Keshmiri, Thermodynamic modeling and performance analysis of photovoltaic-thermal collectors integrated with phase change materials: Comprehensive energy and exergy analysis, Results in Engineering 22 (2024) 102277.
[3] F. Yi, J. E, B. Zhang, H. Zuo, K. Wei, J. Chen, H. Zhu, H. Zhu, Y. Deng, Effects analysis on heat dissipation characteristics of lithium-ion battery thermal management system under the synergism of phase change material and liquid cooling method, Renewable Energy 181 (2022) 472-489.
[4] G.-Z. Yin, A.M. López, I. Collado, A. Vázquez-López, X. Ao, J. Hobson, S.G. Prolongo, D.-Y. Wang, MXene multi-functionalization of polyrotaxane based PCMs and the applications in electronic devices thermal management, Nano Materials Science (2024).
[5] A. Belazreg, A. Abderrahmane, N.A. Qasem, N. Sene, S. Mohammed, O. Younis, K. Guedri, N. Nasajpour-Esfahani, D. Toghraie, Effect of Y-shaped fins on the performance of shell-and-tube thermal energy storage unit, Case Studies in Thermal Engineering 40 (2022) 102485.
[6] F. Ren, J. Du, Y. Cai, J. Guo, Y. Liu, D. Zhang, M. Li, Study on thermal performance of a new optimized snowflake longitudinal fin in vertical latent heat storage, Journal of Energy Storage 50 (2022) 104165.
[7] Q. Zhu, P.J. Ong, S.H.A. Goh, R.J. Yeo, S. Wang, Z. Liu, X.J. Loh, Recent advances in graphene-based phase change composites for thermal energy storage and management, Nano Materials Science 6(2) (2024) 115-138.
[8] M. Al-Jethelah, S.H. Tasnim, S. Mahmud, A. Dutta, Nano-PCM filled energy storage system for solar-thermal applications, Renewable energy 126 (2018) 137-155.
[9] S. Ebadi, S.H. Tasnim, A.A. Aliabadi, S. Mahmud, Melting of nano-PCM inside a cylindrical thermal energy storage system: Numerical study with experimental verification, Energy Conversion and Management 166 (2018) 241-259.
[10] J.M. Mahdi, S. Lohrasbi, D.D. Ganji, E.C. Nsofor, Simultaneous energy storage and recovery in the triplex-tube heat exchanger with PCM, copper fins and Al2O3 nanoparticles, Energy Conversion and Management 180 (2019) 949-961.
[11] H.S. Sultan, H.I. Mohammed, N. Biswas, H. Togun, R.K. Ibrahem, J.M. Mahdi, W. Yaïci, A. Keshmiri, P. Talebizadehsardari, Revolutionizing the latent heat storage: Boosting discharge performance with innovative undulated phase change material containers in a vertical shell-and-tube system, Journal of Computational Design and Engineering 11(2) (2024) 122-145.
[12] N.B. Khedher, H. Togun, A.M. Abed, H.I. Mohammed, J.M. Mahdi, R.K. Ibrahem, W. Yaïci, P. Talebizadehsardari, A. Keshmiri, Comprehensive analysis of melting enhancement by circular Y-

shaped fins in a vertical shell-and-tube heat storage system, Engineering applications of computational fluid mechanics 17(1) (2023) 2227682.
[13] W. Zhou, H.I. Mohammed, S. Chen, M. Luo, Y. Wu, Effects of mechanical vibration on the heat transfer performance of shell-and-tube latent heat thermal storage units during charging process, Applied Thermal Engineering 216 (2022) 119133.
[14] H.I. Mohammed, P. Talebizadehsardari, J.M. Mahdi, A. Arshad, A. Sciacovelli, D. Giddings, Improved melting of latent heat storage via porous medium and uniform Joule heat generation, Journal of Energy Storage 31 (2020) 101747.
[15] W. Alruwaili, M. Jadidi, A. Keshmiri, Y. Mahmoudi, Pore-scale conjugate heat transfer analysis of turbulent flow over stochastic open-cell metal foams, International Journal of Thermal Sciences 202 (2024) 109061.
[16] N.B. Khedher, J.M. Mahdi, A. Dulaimi, I.S. Chatroudi, M. Ebrahimnataj Tiji, R.K. Ibrahem, A. Yvaz, P. Talebizadehsardari, On the application of novel arc-shaped fins in a shell-and-tube type of latent heat storage for energy charge enhancement, Journal of Energy Storage 73 (2023) 108697.
[17] A.M. Abdulateef, S. Mat, J. Abdulateef, K. Sopian, A.A. Al-Abidi, Geometric and design parameters of fins employed for enhancing thermal energy storage systems: a review, Renewable and Sustainable Energy Reviews 82 (2018) 1620-1635.
[18] S. Mat, A.A. Al-Abidi, K. Sopian, M.Y. Sulaiman, A.T. Mohammad, Enhance heat transfer for PCM melting in triplex tube with internal–external fins, Energy conversion and management 74 (2013) 223-236.
[19] M.K. Rathod, J. Banerjee, Thermal performance enhancement of shell and tube Latent Heat Storage Unit using longitudinal fins, Applied thermal engineering 75 (2015) 1084-1092.
[20] A.M. Abdulateef, J. Abdulateef, S. Mat, K. Sopian, B. Elhub, M.A. Mussa, Experimental and numerical study of solidifying phase-change material in a triplex-tube heat exchanger with longitudinal/triangular fins, International Communications in Heat and Mass Transfer 90 (2018) 73-84.
[21] R. Hendra, T. Mahlia, H. Masjuki, Thermal and melting heat transfer characteristics in a latent heat storage system using mikro, Applied Thermal Engineering 25(10) (2005) 1503-1515.
[22] V. Safari, B. Kamkari, H. Abolghasemi, Investigation of the effects of shell geometry and tube eccentricity on thermal energy storage in shell and tube heat exchangers, Journal of Energy Storage 52 (2022) 104978.
[23] L. Pu, S. Zhang, L. Xu, Z. Ma, X. Wang, Numerical study on the performance of shell-and-tube thermal energy storage using multiple PCMs and gradient copper foam, Renewable Energy 174 (2021) 573-589.
[24] S.K. Suraparaju, S.K. Natarajan, Experimental investigation of single-basin solar still using solid staggered fins inserted in paraffin wax PCM bed for enhancing productivity, Environmental Science and Pollution Research 28(16) (2021) 20330-20343.

[25] H.R. Mouziraji, M.E. Tiji, A.M. Abed, A.E. Tiji, H.I. Mohammed, J.M. Mahdi, P. Talebizadehsardari, A. Keshmiri, Boosting Solidification Rates in a Triplex-Tube Thermal Storage System Using Circular Fins: Novel Staggered and Inline Fin Arrangements, Heat Transfer Engineering (2024) 1-22.
[26] M.R. Assari, A.J.G. Beik, R. Eydi, H.B. Tabrizi, Thermal-salinity performance and stability analysis of the pilot salt-gradient solar ponds with phase change material, Sustainable Energy Technologies and Assessments 53 (2022) 102396.
[27] M. Fabrykiewicz, J.T. Cieśliński, Effect of Tube Bundle Arrangement on the Performance of PCM Heat Storage Units, Energies 15(24) (2022) 9343.
[28] M. Fadl, P. Eames, Thermal performance analysis of the charging/discharging process of a shell and horizontally oriented multi-tube latent heat storage system, Energies 13(23) (2020) 6193.
[29] M. Esapour, M. Hosseini, A. Ranjbar, R. Bahrampoury, Numerical study on geometrical specifications and operational parameters of multi-tube heat storage systems, Applied Thermal Engineering 109 (2016) 351-363.
[30] M. Rahimi, A. Ranjbar, D. Ganji, K. Sedighi, M. Hosseini, R. Bahrampoury, Analysis of geometrical and operational parameters of PCM in a fin and tube heat exchanger, International Communications in Heat and Mass Transfer 53 (2014) 109-115.
[31] X. Yang, Z. Lu, Q. Bai, Q. Zhang, L. Jin, J. Yan, Thermal performance of a shell-and-tube latent heat thermal energy storage unit: Role of annular fins, Applied energy 202 (2017) 558-570.
[32] I. Ait Laasri, N. Es-sakali, M. Charai, M.O. Mghazli, A. Outzourhit, Recent progress, limitations, and future directions of macro-encapsulated phase change materials for building applications, Renewable and Sustainable Energy Reviews 199 (2024) 114481.
[33] I.A. Laasri, N. Es-sakali, A. Outzourhit, M.O. Mghazli, Evaluation of phase change materials for a light-weight building in Morocco: Effect of building's volume, window orientation & infiltration, Energy and Built Environment 5(6) (2024) 863-877.
[34] I. Ait Laasri, M. Charai, M.O. Mghazli, A. Outzourhit, Energy performance assessment of a novel enhanced solar thermal system with topology optimized latent heat thermal energy storage unit for domestic water heating, Renewable Energy 224 (2024) 120189.
[35] I. Ait Laasri, Z. Elmaazouzi, M.E. Alami, A. Outzourhit, E.G. Bennouna, Improvement of melting performance in a longitudinal finned latent heat thermal energy storage unit, Energy Storage 6(1) (2024) e510.
[36] R. GmbH, Product Information, data sheet of RT70HC
[37] A. Egea, J.P. Solano, J. Pérez-García, A. García, Solar-driven melting dynamics in a shell and tube thermal energy store: An experimental analysis, Renewable Energy 154 (2020) 1044-1052.
[38] P. Talebizadeh Sardari, G.S. Walker, M. Gillott, D. Grant, D. Giddings, Numerical modelling of phase change material melting process embedded in porous media: Effect of heat storage size,

Proceedings of the Institution of Mechanical Engineers, Part A: Journal of Power and Energy (2019) 0957650919862974.
[39] J.M. Mahdi, E.C. Nsofor, Melting enhancement in triplex-tube latent heat energy storage system using nanoparticles-metal foam combination, Applied Energy 191 (2017) 22-34.
[40] A. Fluent, Ansys Fluent 2020 R1-Theory Guide; User's Guide, Canonsburg, PA, USA (2020).
[41] A. Shahsavar, A. Shaham, P. Talebizadehsardari, Wavy channels triple-tube LHS unit with sinusoidal variable wavelength in charging/discharging mechanism, International Communications in Heat and Mass Transfer 107 (2019) 93-105.
[42] P. Wang, X. Wang, Y. Huang, C. Li, Z. Peng, Y. Ding, Thermal energy charging behaviour of a heat exchange device with a zigzag plate configuration containing multi-phase-change-materials (m-PCMs), Applied energy 142 (2015) 328-336.
[43] M. Esapour, M. Hosseini, A. Ranjbar, Y. Pahamli, R. Bahrampoury, Phase change in multi-tube heat exchangers, Renewable Energy 85 (2016) 1017-1025.
[44] W.-B. Ye, D.-S. Zhu, N. Wang, Numerical simulation on phase-change thermal storage/release in a plate-fin unit, Applied Thermal Engineering 31(17) (2011) 3871-3884.
[45] E. Assis, L. Katsman, G. Ziskind, R. Letan, Numerical and experimental study of melting in a spherical shell, International Journal of Heat and Mass Transfer 50(9) (2007) 1790-1804.
[46] A.A. Al-Abidi, S. Mat, K. Sopian, M.Y. Sulaiman, A.T. Mohammad, Internal and external fin heat transfer enhancement technique for latent heat thermal energy storage in triplex tube heat exchangers, Applied Thermal Engineering 53(1) (2013) 147-156.
[47] A.A. Al-Abidi, S. Mat, K. Sopian, M.Y. Sulaiman, A.T. Mohammad, Experimental study of melting and solidification of PCM in a triplex tube heat exchanger with fins, Energy and Buildings 68 (2014) 33-41.
[48] S. Yang, H. Oliver Gao, F. You, Model predictive control in phase-change-material-wallboard-enhanced building energy management considering electricity price dynamics, Applied Energy 326 (2022) 120023.
[49] D. Jalili, M. Jadidi, A. Keshmiri, B. Chakraborty, A. Georgoulas, Y. Mahmoudi, Transfer learning through physics-informed neural networks for bubble growth in superheated liquid domains, International Journal of Heat and Mass Transfer 232 (2024) 125940.
[50] D. Jalili, S. Jang, M. Jadidi, G. Giustini, A. Keshmiri, Y. Mahmoudi, Physics-informed neural networks for heat transfer prediction in two-phase flows, International Journal of Heat and Mass Transfer 221 (2024) 125089.